

BROWNIAN MOTION OF BLACK HOLES IN DENSE NUCLEI

DAVID MERRITT

Department of Physics, Rochester Institute of Technology, Rochester, NY 14623, USA

PETER BERCZIK

Astronomisches Rechen-Institut, Zentrum für Astronomie Univ. Heidelberg, Monchhofstrasse 12-14, 69120 Heidelberg, Germany *and*
 Main Astronomical Observatory, National Academy of Sciences of Ukraine, Zabolotnoho Str., 27, 03680, Kiev, Ukraine

FREDERIK LAUN

Abteilung Medizinische Physik in der Radiologie, Deutsches Krebsforschungszentrum, Im Neuenheimer Feld 280, D-69120 Heidelberg, Germany
Draft version 20th March 2022

Abstract

We evaluate the Brownian motion of a massive particle (“black hole”) at the center of a galaxy using N -body simulations. Our galaxy models have power-law central density cusps like those observed at the centers of elliptical galaxies. The simulations show that the black hole achieves a steady-state kinetic energy that is substantially different than would be predicted based on the properties of the galaxy model in the absence of the black hole. The reason appears to be that the black hole responds to stars whose velocities have themselves been raised by the presence of the black hole. Over a wide range of density slopes and black hole masses, the black hole’s mean kinetic energy is equal to what would be predicted under the assumption that it is in energy equipartition with stars lying within a distance $\sim r_h/2$ from it, where r_h is the black hole’s influence radius. The dependence of the Brownian velocity on black hole mass is approximately $\langle V^2 \rangle \propto M_{BH}^{-1/(3-\gamma)}$ with γ the power-law index of the stellar density profile, $\rho \propto r^{-\gamma}$. This is less steep than the M_{BH}^{-1} dependence predicted in a model where the effect of the black hole on the stellar velocities is ignored. The influence of a stellar mass spectrum on the black hole’s Brownian motion is also evaluated and found to be consistent with predictions from Chandrasekhar’s theory. We use these results to derive a probability function for the mass of the Milky Way black hole based on a measurement of its proper motion velocity. Interesting constraints on M_{BH} will require a velocity resolution exceeding 0.5 km s^{-1} .

Subject headings: stellar dynamics, galaxies: nuclei, black holes

1. INTRODUCTION

A massive black hole at the center of a galaxy undergoes a random walk in momentum space as its motion is perturbed by gravitational encounters with nearby stars. The expected amplitude of this “gravitational Brownian motion” is

$$\langle V^2 \rangle \approx 3 \frac{m}{M} \sigma^2 \approx (0.1 \text{ km s}^{-1})^2 \left(\frac{m}{M_\odot} \right) \left(\frac{M}{3 \times 10^6 M_\odot} \right)^{-1} \times \left(\frac{\sigma}{100 \text{ km s}^{-1}} \right)^2 \quad (1)$$

where M and m are the mass of the black hole and a typical star respectively and σ is the 1D stellar velocity dispersion; the brackets denote a time average. Equation (1) follows from assuming that the average kinetic energy of the black hole is equal to that of the stars. Gravitational Brownian motion is potentially interesting for a number of reasons: as a means to constrain black hole masses (e.g. Backer & Sramek (1999); Reid et al. (1999, 2003)); as a mechanism for displacing black holes from their otherwise central locations in galaxies (e.g. Bahcall & Wolf (1976)); and as a possible source of enhancement in the rate of supply of stars to the black hole (e.g. Young (1980)).

The approximate validity of equation (1) has been confirmed in a number of numerical studies (Miller 1992; Taga & Iye 1998; Milosavljević & Merritt 2001; Chatterjee, Hernquist, & Loeb 2002a,b; Dorband, Hemsendorf, & Merritt

2003; Chatterjee, Hernquist, & Loeb 2003; Makino & Funato 2004). With two exceptions however (Milosavljević & Merritt 2001; Dorband, Hemsendorf, & Merritt 2003), these studies have been based on galaxy models with large, low-density cores, very different from the dense, $\rho \sim r^{-\gamma}$ nuclei observed at the centers of the galaxies known to harbor supermassive black holes. Furthermore the black hole particle is often introduced into the simulations in a non-self-consistent way: first a black-hole-free model is constructed, then the black hole is added, which causes the galaxy model to evolve away from its initial state as the stellar motions respond to the suddenly deepened potential (e.g. Chatterjee, Hernquist, & Loeb (2002a,b)). These practices complicate the interpretation of the numerical simulations and make it difficult to derive predictions about the expected behavior of black holes in real nuclei. For example, the quantity σ that appears in equation (1) is well defined at the center of a low-density galaxy containing no black hole, but in a real galaxy, σ is a strong function of radius, due both to the inhomogeneity of the galaxy and to the presence of the black hole itself.

These considerations motivated us to undertake a new series of numerical studies of gravitational Brownian motion. Our primary goal was to evaluate the validity of the equipartition assumption for black holes at the centers of galaxy models with realistically high central densities. We carried out a set of N -body integrations similar in character to those described by Dorband, Hemsendorf, & Merritt (2003), but with a wider

range of galaxy models and, in some cases, with a spectrum of stellar masses. All of the galaxy models have a power-law dependence of stellar density on radius near the center, and the initial stellar velocities were generated from a distribution function that accounts for the gravitational force from the “black hole”; hence, the models are in a precisely equilibrium state at time zero.

Our results can be summarized in a surprisingly simple way: the black hole reaches a state of energy equipartition with the stars lying at distances $\lesssim r_h/2$ from it, where r_h is the black hole’s gravitational influence radius (a precise definition of r_h is given below). By definition, stars within r_h are moving largely in response to the gravitational force from the black hole; hence, the black hole’s Brownian motion is determined by the velocities of stars which themselves have been raised by the presence of the black hole! One consequence is that the black hole’s rms velocity does not drop as steeply with black hole mass as the $M^{-1/2}$ dependence predicted by equation (1). Another is that $\langle V^2 \rangle$ can be substantially different – higher or lower – than the value predicted by equation (1) if σ is measured outside of the black hole’s influence radius.

The properties of our galaxy models and the details of the N -body integrations are presented in §2 and §3. The predictions of Chandrasekhar’s theory of stellar encounters are reviewed in §4; as we point out there, Chandrasekhar’s theory is essentially local in character and does not make useful predictions about the expected value of $\langle V^2 \rangle$ in realistic, inhomogeneous galaxies. Nevertheless the theory does say something definite about the relation between $\langle V^2 \rangle$ in the single- and multi-mass cases. Results from the N -body integrations are presented in §5 (single stellar mass) and §6 (mass spectrum). In §7, we use our results to predict the expected amplitude of the Brownian motion for the Milky Way black hole, and show how a measurement of its velocity, or determination of an upper limit, can be converted into a probability function for its mass.

2. GALAXY MODEL

Supermassive black holes are observed at the centers of early-type galaxies and the bulges of spiral galaxies. The luminosity profiles of these systems are well represented as power laws in the radius at distances from the black hole less than $\sim r_b$, the break radius. (So-called “core” galaxies also have luminosity profiles that are power laws in the space density, but with indices less than one.) We adopted Dehnen’s (1993) density profile for our galaxy models:

$$\rho(r) = \frac{(3-\gamma)M_{\text{gal}}}{4\pi} \frac{a}{r^\gamma(r+a)^{4-\gamma}} \quad (2)$$

where $\rho(r)$ is the stellar mass density, M_{gal} is the total mass in stars, a is the scale length (roughly speaking, the break radius) and γ is the logarithmic slope of the central density cusp.

To this galaxy model was added a central point of mass M representing the black hole. For our purposes, it was crucial that the initial model be in a steady state, so that any time dependence could be attributed to perturbations resulting from the finite- N realization of the model, and not to ill-defined departures from equilibrium. To achieve this, the initial velocities of the stars were generated from the unique, isotropic phase-space distribution function that reproduces the Dehnen density law in the smooth combined potential of the stars and the black hole particle (Tremaine et al. 1994). This distribution function is non-negative for $\gamma \geq 0.5$ in the presence of a central point mass; we considered values of γ in the range

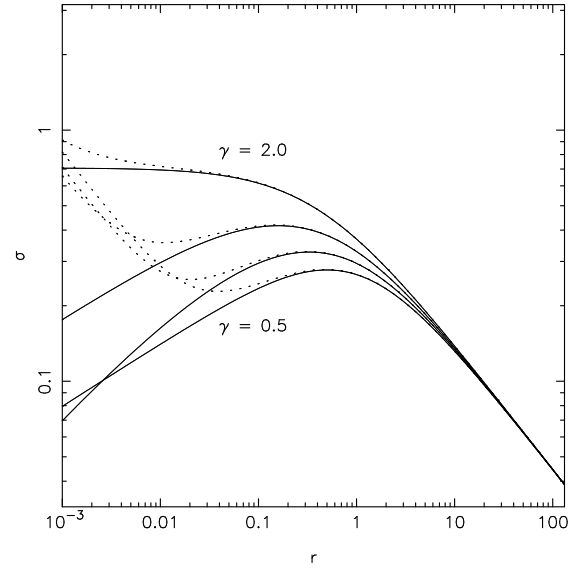


FIG. 1.— 1D velocity dispersion profiles for Dehnen models without central black holes (solid lines) and with central black holes of mass $M = 10^{-3}M_{\text{gal}}$ (dashed lines). γ increases downward, from $\gamma = 2$ to $\gamma = (1.5, 1.0, 0.5)$.

TABLE 1
DEHNEN MODEL
PARAMETERS

γ	σ_p	r_p
0.5	0.2775	0.500
1.0	0.3270	0.330
1.5	0.4164	0.159
2.0	0.7071	0

$0.5 \leq \gamma \leq 2$. The black hole particle was given zero velocity initially.

Unless otherwise indicated, we present our results in units such that $G = a = M_{\text{gal}} = 1$. In these units, M represents the ratio of the black hole mass to the total mass in stars. In real galactic spheroids, this ratio is approximately 10^{-3} , although with some scatter (Merritt & Ferrarese 2001; Marconi & Hunt 2003). We considered values of M in the range $10^{-4} \leq M \leq 10^{-1}$. The lower limit is fixed by the requirement that the black hole particle be appreciably more massive than the star particles.

Figure 1 shows the (1D) radial velocity dispersion profile $\sigma(r)$ for Dehnen models with $M = 0$ and $M = 10^{-3}$. In the absence of a black hole and for $\gamma \neq 2$, $\sigma(r)$ peaks at a non-zero radius; furthermore the peak value is nearly unaffected by the presence of a black hole of mass $10^{-3}M_{\text{gal}}$. Since the amplitude of the Brownian motion of the black hole is expected to scale with the stellar velocity dispersion, it is of interest to define a characteristic value of σ near the centers of these models. A natural choice is $\sigma_p(\gamma)$, the peak value of σ in a model without a central black hole. We define r_p as the radius at which $\sigma(r) = \sigma_p$. Table 1 gives values of σ_p and r_p as functions of γ .

Most of our N -body integrations were carried out on models containing stars of equal mass. We also carried out some integrations of models in which the stars had a range of masses. The stellar masses in the multi-mass integrations were gener-

ated randomly from the mass function

$$n(m)dm \propto m^{-(1+\alpha)}dm \quad (3)$$

with $\alpha = 1.35$, the Salpeter (1955) value. Given a mean mass $\bar{m} = M_{\text{gal}}/N$ with N the number of particles, the mass spectrum is determined by equation (3) and by m_1/m_2 , the ratio of smallest to largest stellar mass. We used $m_1/m_2 = 0.01$.

3. N-BODY INTEGRATIONS

All N -body integrations were carried out using a high-accuracy, direct-summation, parallel N -body code (Berczik et al. 2005) on two supercomputers incorporating special-purpose GRAPE (Fukushige et al. 2005) accelerator boards: gravitySimulator¹ and GRACE.² Particle positions were advanced using the fourth-order Hermite scheme, with discretized individual time steps chosen according to the criterion of Makino & Aarseth (1992), and a time-step accuracy parameter $\eta = 0.01$. All integrations used $N = 10^6$ “star” particles. Inter-particle forces were softened using the standard expression,

$$\mathbf{F}_{12} = -Gm_1m_2 \frac{\mathbf{r}_1 - \mathbf{r}_2}{(|\mathbf{r}_1 - \mathbf{r}_2|^2 + \varepsilon^2)^{3/2}}; \quad (4)$$

the same softening length was assigned to star and to black hole particles.

In what follows, it is argued that the black hole’s Brownian motion is determined in large part by perturbations from stars that lie within its influence radius r_h , defined (in a slightly non-standard way) as the radius containing a mass in stars equal to twice the black hole mass. This means that the softening length should be small compared with r_h , and in particular, small enough that the macroscopic structure of the galaxy model does not change at $r \lesssim r_h$ due to inaccurate representation of the potential. Table 2 gives values of r_h for each set of (M, γ) values considered here. We verified that a softening length of $\varepsilon = 10^{-4}$ resulted in no discernible evolution in any of the models with $\gamma \leq 1.5$ even at radii $\lesssim 0.1r_h$. Furthermore, as shown below (Fig. 4), our results for the $\gamma = 1.5$ models using this value of ε were essentially indistinguishable from those obtained in the earlier study of Dorband et al. (2003) who used a code with zero softening. For the models with $\gamma = 2$ and small M , some evolution at $r < r_h$ was observed for $\varepsilon = 10^{-4}$ and we conservatively adopted the smaller softening length $\varepsilon = 10^{-5}$ for these models.

Even if ε is small enough to accurately reproduce the small-scale structure of the galaxy models, evolution can still occur after a sufficiently long time as the star particles exchange energy. In the equal-mass case, the relevant time scale is the two-body relaxation time,

$$T_r(r) = \frac{0.34\sigma(r)^3}{\rho(r)mG^2 \ln \Lambda} \quad (5)$$

(Spitzer 1987), with $\ln \Lambda$ the Coulomb logarithm. A collisional steady state, $\rho \propto r^{-7/4}$, is reached near the black hole in a time $\sim T_r(r_h)$ (Bahcall & Wolf 1976). Table 2 gives estimates of $T_r(r_h)$, computed using $\Lambda = r_h\sigma^2(r_h)/2Gm_*$ (Preto, Merritt & Spurzem 2004). The short relaxation times in models with large γ and small M restricts how long these models can be integrated before their structure changes.

TABLE 2
SINGLE-MASS N -BODY INTEGRATIONS ($N = 10^6$)

M	γ	r_h	$T_r(r_h)$	$\langle V^2 \rangle$	η
1×10^{-1}	0.5	1.11	6.4×10^4	6.72×10^{-6}	2.91
	1.0	8.09×10^{-1}	4.3×10^4	7.60×10^{-6}	2.37
	1.5	5.20×10^{-1}	2.4×10^4	1.90×10^{-5}	3.65
	2.0	2.50×10^{-1}	9.7×10^3	8.19×10^{-5}	5.46
3×10^{-2}	0.5	4.80×10^{-1}	1.4×10^4	8.40×10^{-6}	1.09
	1.0	3.24×10^{-1}	8.2×10^3	2.04×10^{-5}	1.91
	1.5	1.81×10^{-1}	3.6×10^3	5.74×10^{-5}	3.31
	2.0	6.38×10^{-2}	8.4×10^2	2.73×10^{-4}	5.46
1×10^{-2}	0.5	2.64×10^{-1}	5.5×10^3	2.08×10^{-5}	0.902
	1.0	1.65×10^{-1}	2.6×10^3	5.49×10^{-5}	1.71
	1.5	7.95×10^{-2}	8.2×10^2	1.24×10^{-4}	2.39
	2.0	2.04×10^{-2}	1.0×10^2	7.00×10^{-4}	4.67
3×10^{-3}	0.5	1.48×10^{-1}	2.4×10^3	8.87×10^{-5}	1.152
	1.0	8.40×10^{-2}	8.3×10^2	9.34×10^{-5}	0.873
	1.5	3.41×10^{-2}	1.7×10^2	2.40×10^{-4}	1.39
	2.0	6.03×10^{-3}	1.1×10^1	2.13×10^{-3}	4.26
1×10^{-3}	0.5	9.08×10^{-2}	1.2×10^3	1.03×10^{-4}	0.445
	1.0	4.68×10^{-2}	3.1×10^2	1.96×10^{-4}	0.600
	1.5	1.61×10^{-2}	4.1×10^1	5.08×10^{-4}	0.977
	2.0	2.00×10^{-3}	1.4×10^0	5.42×10^{-3}	3.61
3×10^{-4}	0.5	5.42×10^{-2}	6.6×10^2	1.23×10^{-4}	0.159
	1.0	2.51×10^{-2}	1.1×10^2	3.58×10^{-4}	0.335
	1.5	7.16×10^{-3}	8.5×10^0	1.22×10^{-3}	0.705
	2.0	6.00×10^{-4}	1.6×10^{-1}	–	–

We adopted the following integration times in model units:

$$\begin{aligned} \gamma = 0.5, T &= 8 \\ \gamma = 1.0, T &= 4 \\ \gamma = 1.5, T &= 2 \\ \gamma = 2.0, T &= 1. \end{aligned}$$

As Table 2 shows, the model with $(\gamma, M) = (2.0, 3 \times 10^{-4})$ has $T_r(r_h) \approx 0.16$, substantially shorter than the adopted integration time, and so short that it would be difficult to get good “statistics” on the black hole’s Brownian motion in a time $\lesssim T_r$. Accordingly, we omit the results from this integration in the Table and in the discussion that follows.

When evaluating the amplitude of the black hole’s motion, a possible concern is any steady component of its velocity due to a net drift of the N -body system’s center of mass. The amplitude of the drift is expected to be of order $V_{\text{drift}} \approx VN^{-1/2}$, where V is a characteristic internal (stellar) velocity. This may be compared with the expected rms velocity characterizing the black hole’s Brownian motion, which is $\sim \sigma N^{-1/2}(M/M_{\text{gal}})^{-1/2}$. The latter is larger than the former by \sim an order of magnitude even for the largest black hole mass that we considered, $M/M_{\text{gal}} = 0.1$. We inspected the configuration-space motion of the black hole particles in all of our integrations; in few if any of the cases could we see evidence of a steady drift component to the motion, and when it was present, it was too small to significantly affect the estimates of $\langle V^2 \rangle$. Hence we ignore V_{drift} in what follows.

The situation is a little different in the multi-mass runs, since a single massive particle of mass m_* can spiral into the center in a time of order $\sim (\bar{m}/m_*)T_r$ where \bar{m} is the mean stellar mass. The particle masses in these models were generated randomly and a massive particle could find itself initially on an orbit for which the dynamical friction time is short.

¹ See <http://www.cs.rit.edu/~grapecluster/clusterInfo/grapeClusterInfo.shtml>.

² See <http://www.ari.uni-heidelberg.de/grace>.

While this effect is a potential source of bias in the multi-mass runs, the multi-mass integrations were shorter than the single-mass integrations, and we found no evidence of a significant time dependence in the Lagrange radii, nor in the black hole's $\langle V^2 \rangle$, that would suggest a systematic change in the stellar distribution over the course of the integrations. In any case, the run-to-run variation in $\langle V^2 \rangle$ due to different random realizations of the same model were so large that they probably swamped this effect (§6).

4. EXPECTATIONS FROM LOCAL THEORY

Existing theories of gravitational Brownian motion are too idealized to make clear predictions about the amplitude of the Brownian motion in our models, for several reasons. First, the black hole is massive enough that it modifies the gravitational potential as it moves. Second, particles in tightly-bound orbits around the black hole will increase its effective mass. Third, the properties of the stellar background, e.g. density and velocity dispersion, are strong functions of distance from the black hole. Standard encounter theory (e.g. Spitzer 1987) approximates the stellar background as homogeneous and time-independent and ignores the effects of a massive particle on its surroundings.

The predictions of idealized theory are nevertheless useful as a baseline against which to compare the N -body results. Using the Fokker-Planck equation, the steady-state velocity distribution of a massive particle that moves in response to perturbations from an infinite and homogeneous distribution of background stars is

$$f(V) = f_0 e^{-3V^2/2\langle V^2 \rangle}, \quad \langle V^2 \rangle = \frac{3C}{2A} \quad (6)$$

where $\langle V^2 \rangle$ is the mean square (3D) velocity of the black hole and A and C characterize the low-velocity limit of the black hole's diffusion coefficients due to encounters with stars:

$$\langle \Delta v_{\parallel} \rangle = -AV + BV^3 \dots, \quad (7a)$$

$$\langle \Delta v_{\parallel}^2 \rangle = C + DV^2 \dots \quad (7b)$$

(e.g. Merritt 2001). The latter depend on the phase-space number density of stars $f_{\star} = f_{\star}(\mathbf{v}, \mathbf{r})$. If f_{\star} is assumed to be isotropic in velocity space, then

$$A = \frac{32}{3} \pi^2 G^2 M m n \int_0^{\infty} \frac{dv}{v} f_{\star}(v) \frac{p_{\max}^2 v^4 / G^2 M^2}{1 + p_{\max}^2 v^4 / G^2 M^2}, \quad (8a)$$

$$C = \frac{16}{3} \pi^2 G^2 m^2 n \int_0^{\infty} dv v f_{\star}(v) \ln \left(1 + \frac{p_{\max}^2 v^4}{G^2 M^2} \right) \quad (8b)$$

(Merritt 2005). Here m is the stellar mass, n is the stellar number density, and p_{\max} is the maximum effective impact parameter in Chandrasekhar's theory. In the special case of a Maxwellian distribution of field star velocities, $f_{\star}(v) = f_0 e^{-v^2/2\sigma^2}$ and

$$A = \frac{4\sqrt{2\pi}}{3} \frac{G^2 M m n}{\sigma^3} F(R), \quad C = \frac{8\sqrt{2\pi}}{3} \frac{G^2 m^2 n}{\sigma} F(R) \quad (9a)$$

$$F(R) \equiv \frac{1}{2} \int_0^{\infty} dz e^{-z} \ln(1 + 4R^2 z^2), \quad R \equiv \frac{p_{\max} \sigma^2}{GM} \quad (9b)$$

and

$$\langle V^2 \rangle = \frac{3C}{2A} = 3 \left(\frac{m}{M} \right) \sigma^2. \quad (10)$$

The predicted $\langle V^2 \rangle$ is independent of p_{\max} in this case and is equal to the “equipartition” value.

The velocity distribution at the center of the Dehnen models is not precisely Maxwellian. While it is straightforward to derive expressions for A and C for non-Maxwellian f_{\star} 's (Merritt 2005), a more serious problem then presents itself. The velocity dispersion at the center of a Dehnen model is *zero* in the absence of a black hole (in all models excepting those with $\gamma = 0$ or 2); and it is *infinite* when the effect of the black hole on the stellar motions is included (Figure 1). Thus equations like (10), naively applied, predict either $\langle V^2 \rangle = 0$ or $\langle V^2 \rangle = \infty$, depending on whether or not the black hole's influence on the equilibrium stellar model is taken into account, and of course neither result is physically reasonable. The local theory fails because the Dehnen models (like real galaxies) are inhomogeneous, both in their density and velocity structure, and because the presence of the black hole strongly influences even the equilibrium stellar velocity distribution in its vicinity.

Local theory does make one potentially useful prediction. If the massive particle's diffusion coefficients are re-derived for the case of a spectrum of perturber masses, one can relate the predicted $\langle V^2 \rangle$ to its value in the case of a single perturber mass. Define the mass function such that $n(m)dm$ is the number density of stars in mass range m to $m + dm$, and assume that the velocity distribution is the same for all mass groups. In the multi-mass case,

$$A_{mm} = \frac{32\pi^2}{3} G^2 M \left[\int_{m_1}^{m_2} n(m) m dm \right] \int_0^{\infty} \frac{dv}{v} f_{\star}(v) \frac{p_{\max}^2 v^4 / G^2 M^2}{1 + p_{\max}^2 v^4 / G^2 M^2}, \quad (11a)$$

$$C_{mm} = \frac{16\pi^2}{3} G^2 \left[\int_{m_1}^{m_2} n(m) m^2 dm \right] \int_0^{\infty} dv v f_{\star}(v) \log \left(1 + \frac{p_{\max}^2 v^4}{G^2 M^2} \right). \quad (11b)$$

The mean square velocity of the black hole in the multi-mass case, for a Maxwellian distribution of field-star velocities, is therefore predicted to be

$$\langle V^2 \rangle_{mm} = \left(\frac{3C}{2A} \right)_{mm} = 3 \left(\frac{\tilde{m}}{M} \right) \sigma^2, \quad (12)$$

i.e. \tilde{m}/m times its value in the case of a single perturber mass m , where the variable \tilde{m} is

$$\tilde{m} \equiv \frac{\int n(m) m^2 dm}{\int n(m) m dm}. \quad (13)$$

This prediction will be tested below via N -body integrations.

Brownian motion results in a time-dependent displacement of the black hole from its otherwise central location in a galaxy. The N -body integrations presented here were judged to be too short to extract useful information about the amplitude of this displacement (as opposed to the velocity), and in what follows, we focus on changes in velocity. We will return to the question of Brownian *displacements* in a subsequent paper.

5. RESULTS: SINGLE-MASS MODELS

Figure 2 illustrates the time dependence of the black hole's velocity in a representative set of integrations. The “frequency” of the motion increases with increasing γ , as expected, since the period of small oscillations about the potential center is smaller for larger γ . However none of these plots exhibits the quasi-harmonic motion characteristic of particles

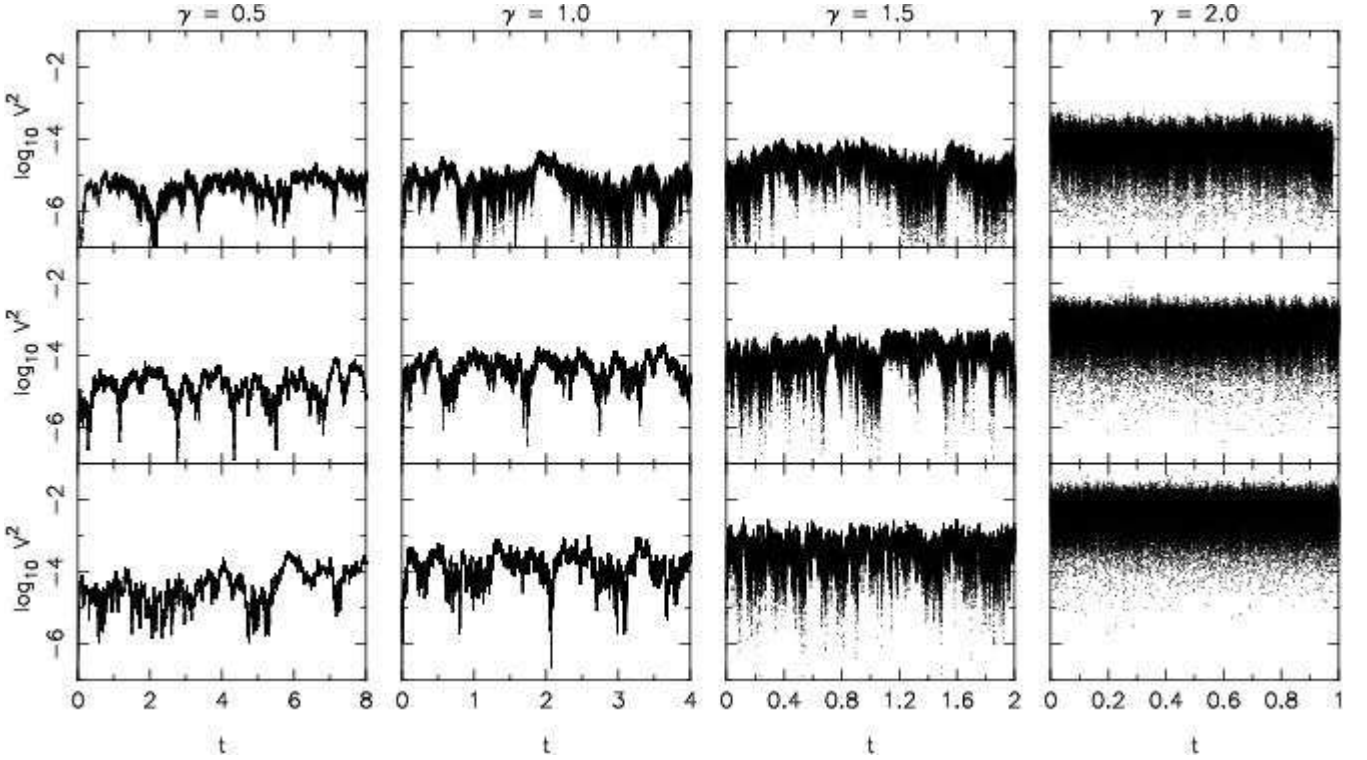


FIG. 2.— Time dependence of black hole velocity in a set of integrations. From top to bottom, the black hole mass is 10^{-1} , 10^{-2} and 10^{-3} in units of the galaxy mass.

wandering in a constant-density core (e.g. Miller & Smith 1992).

Brownian motion of a particle in a classical gas obeys a Maxwell-Boltzmann distribution. As shown above (§4), the same is predicted by the Fokker-Planck equation for a massive particle moving in response to gravitational perturbations in an infinite homogeneous background of stars, as long as the dynamical friction coefficient obeys Hooke's law at low velocities. However the equations derived above embody many approximations that are violated in the N -body models and in real galaxies. Hence it is interesting to directly compute the time-averaged velocity distribution of the massive particle in the N -body integrations. Figure 3 shows $N(V)$ for integrations with $M = 10^{-3}$ and four different values of γ . The velocity of the black hole particle was sampled at fixed intervals, ranging from $\Delta t = 0.002$ for $\gamma = 0.5$ to $\Delta t = 0.00003$ for $\gamma = 2.0$.

The empirical velocity distributions in Figure 3 are compared with the Maxwell-Boltzmann distribution,

$$N(V)dV = 4\pi V^2 (2\pi\langle V^2 \rangle/3)^{-3/2} \exp(-3V^2/2\langle V^2 \rangle) dV. \quad (14)$$

The quantity $\langle V^2 \rangle$ in equation (14) was computed directly from the time series of stored velocities; it was not adjusted to increase the goodness of fit of equation (14) to the measured $N(V)$. Nevertheless, the fit of the measured $N(V)$'s to the Maxwell-Boltzmann distribution is clearly good, and nearly perfect in the case of $\gamma = 2$; in this model, the black hole particle experienced the largest number of velocity updates. We verified that the bumps and wiggles in the plots of $N(V)$ for $\gamma = 0.5$ and $\gamma = 1.0$ were essentially random, by constructing $N(V)$ separately for the first and second halves of the integration intervals.

If we assume that the time-averaged $N(V)$ is well described

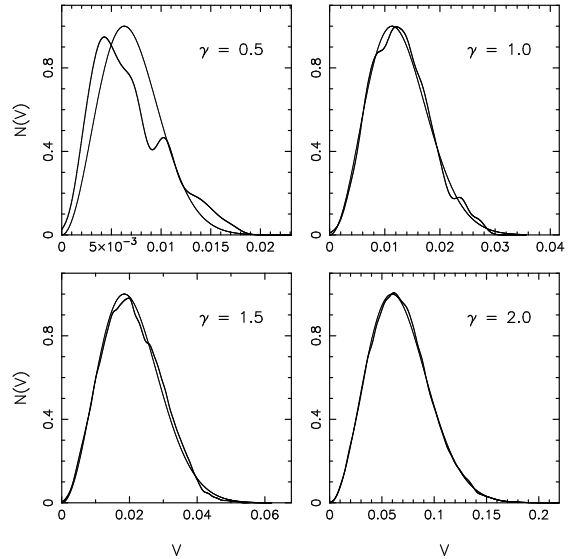


FIG. 3.— Measured distribution of black hole velocities in four integrations with $M = 10^{-3}$. Thin curves show Maxwell-Boltzmann distributions, computed as described in the text.

by the Maxwell-Boltzmann distribution, then the only quantity required to specify $N(V)$ is $\langle V^2 \rangle$. We expect $\langle V^2 \rangle$ to be close to the “energy equipartition” value at which the time-averaged kinetic energy of the black hole equals the mean kinetic energy of nearby stars. We write this as

$$\langle V^2 \rangle = 3\eta \frac{m}{M} \sigma_p^2 \quad (15)$$

where σ_p is the peak value of the 1D stellar velocity disper-

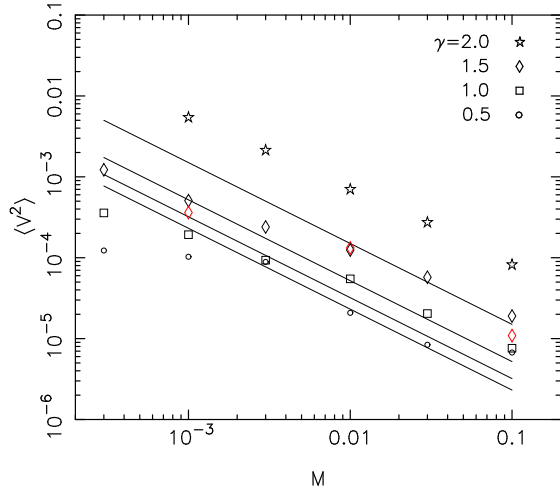


FIG. 4.— Mean square velocity of the black hole particle as given in Table 2 for the various N -body integrations. Lines show the “equipartition” relations, $\eta = 1$. Red diamonds are from Dorband et al. (2003).

TABLE 3
 $\log_{10} \eta =$
 $A + B \log_{10} M$

γ	A	B
0.5	0.844	0.420
1.0	0.801	0.345
1.5	0.934	0.307
2.0	0.853	0.093

sion, as defined in §2, and η is a parameter whose value is expected to be close to one. Values of $\langle V^2 \rangle$ are given in Table 2, and plotted in Figures 4 and 5 as functions of M and γ . These values were computed by sampling the stored velocities at small fixed intervals. The lines in Figure 4 show the “equipartition” relations, $\eta = 1$.

Two results are apparent from Figures 4 and 5.

1. There is a clear dependence of $\langle V^2 \rangle$ on M , although less steep than the expected $\langle V^2 \rangle \propto M^{-1}$ dependence.

2. For a fixed black hole mass, the fractional discrepancy between the measured $\langle V^2 \rangle$ and the “equipartition” value is an increasing function of γ .

Another way to present these results is to interpret equation (15) as defining the parameter η , which then measures departures from “equipartition” as a function of M and γ . Figure 6 plots η , so defined, for these integrations; the η values are also given in Table 2. As the two previous figures indicated, η increases systematically with M and γ , reaching values as large as ~ 5.5 for $(M, \gamma) = (0.1, 2.0)$. For small (M, γ) , η drops below one, to values as low as ~ 0.2 .

The dependence of $\log \eta$ on $\log M$ is nearly linear for fixed γ (Figure 6). We carried out least-squares fits to find the coefficients of $\log_{10} \eta \approx A + B \log_{10} M$. The results of the fits are given in Table 3. These results imply that – in a galaxy with otherwise fixed properties – the mean square velocity of the black hole scales as $\sim M^{-0.6}$ in low-density nuclei and $\sim M^{-0.9}$ in high-density nuclei. Ignoring the effect of the black hole on the stellar motions would lead to the prediction $\langle V^2 \rangle \propto M^{-1}$.

There is a natural way to understand these results. The

steady-state velocities of the stars in these galaxy models are influenced by the presence of the black hole (Figure 1), very strongly at distances $\lesssim r_h$. The Brownian motion of the black hole depends in turn on perturbations from these fast-moving stars. The more massive the black hole, the hotter the surrounding stellar fluid, and the greater the expected deviation of the black hole’s Brownian velocity from the value that would have been predicted based on the properties of a model with the same density structure but lacking a black hole. These deviations should also be an increasing function of γ , since for larger γ , the number of high-velocity stars near the black hole is larger.

Suppose we assume that the black hole’s kinetic energy is in equipartition with the stars in some region around it. Define $\tilde{\sigma}^2$ to be the 1D, mean square stellar velocity within this region, which has radius \tilde{r} . The black hole’s Brownian velocity would then be

$$\langle V^2 \rangle = 3 \frac{m}{M} \tilde{\sigma}^2, \quad (16)$$

It is understood that $\tilde{\sigma}^2$ in equation (16) includes the effect of the black hole on the equilibrium stellar motions. We might guess, based on the N -body results, that the best choice for \tilde{r} is some multiple of the black hole’s radius of influence r_h , $\tilde{r} = F \times r_h$.

Before testing this hypothesis, we make two remarks.

1. The standard definition of r_h is GM/σ^2 . This definition is adequate for galaxies where $\sigma(r)$ is approximately constant near the center. For the Dehnen models, this is only true for $\gamma = 2$, and it is never true in models containing a central black hole. In §3, we generalized the definition of r_h to be the radius containing a mass in stars equal to twice the black hole mass. Thus, at $r = r_h$, the gravitational force from the black hole is one-half that due to the stars. We retain that definition in what follows.

2. Above we defined $\tilde{\sigma}^2$ as the mean value of σ^2 within some radius, including the effect of the black hole’s gravity on the stellar motions. However for $\gamma \geq 2$, this quantity *diverges* as a function of the lower integration limit, due to the $\sigma^2 \propto r^{-1}$ increase in velocities near the black hole. Nevertheless the divergence is only logarithmic as a function of the lower integration limit when $\gamma = 2$. In our N -body models, a natural choice for the lower integration limit is ϵ , the softening length. We made this choice in what follows.

Figure 6 shows the predictions of equation (16) compared with the N -body data, setting $F = 0.6$, i.e. when $\tilde{\sigma}^2$ is computed as an average within $0.6r_h$. In this plot, the ordinate is the value of η that would have been measured if the black hole’s Brownian velocity were given by equation (16), i.e. $\eta = \tilde{\sigma}^2/\sigma_p^2$. The agreement with the data is quite good, considering the simplicity of the prescription, the wide range in density structure of the models, and the fairly arbitrary definition of r_h . The worst fit is for $\gamma = 0.5$, however these points exhibit a large scatter, probably reflecting that the N -body integration time was barely long enough to provide a robust sampling of the massive particle’s motion (Fig. 2).

Other definitions of \tilde{r} were tried (e.g., a fixed value in model units) but none was found that reproduced the measured values of η so well.

We carried out least-squares fits against the data of Figure 6 to determine the best value of F for each γ . For $\gamma = (0.5, 1, 1.5, 2)$, we found best-fit F ’s of $(0.77, 0.76, 0.52, 0.66)$. The fit to the $\gamma = 2$ data was nearly perfect when the optimal F was used. We conclude that the “black holes” in our simulations are in approximate en-

ergy equipartition with the stars that lie in a sphere of radius $(0.67 \pm 0.10)r_h$ around them. Excluding the rather poor fit for $\gamma = 0.5$, this becomes $(0.65 \pm 0.10)r_h$.

We can develop a simple model that reproduces these results. We suppose that the black hole's motion can be broken into two pieces:

$$\langle V^2 \rangle = \langle V_1^2 \rangle + \langle V_2^2 \rangle. \quad (17)$$

The first piece, $\langle V_1^2 \rangle$, refers to the motion of the center of mass of the system consisting of the black hole and the stars bound to it. The second piece, $\langle V_2^2 \rangle$, is the mean square velocity of the black hole with respect to the center of mass of the bound system.

Our model requires that we first identify which stars are “bound” to the black hole. Clearly, stars with apocenter distances $r_+ \ll r_h$ are bound to the black hole, and stars with $r_+ \gg r_h$ are not. However stars with $r_+ \approx r_h$ can neither be said to be bound or unbound. We will call a star “bound” if

$$r_+ < F' r_h. \quad (18)$$

Here $F' \approx 1$ is a free parameter similar to the factor F defined above. According to this definition, the gravitational force on the “bound” stars comes predominantly from the black hole.

Let the mass in bound stars be M_b . Then the effective mass of the bound system (black hole plus stars) is

$$M_{eff} = M + M_b. \quad (19)$$

The remaining (unbound) stars define a core with some characteristic density and velocity dispersion. Define the latter to be σ_u . We compute σ_u by taking an average over the unbound stars within a region of radius $2F'r_h$.

Given these definitions, the contribution to the black hole's motion from the unbound stars is given by Chandrasekhar's theory (§4):

$$\langle V_1^2 \rangle \approx 3 \frac{m}{M_{eff}} \sigma_u^2. \quad (20)$$

In other words, we expect the bound system, of mass M_{eff} , to act like a single particle in energy equipartition with the unbound stars in the core.

The motion of the black hole with respect to the center of mass of the bound system can be computed by setting

$$M\mathbf{V}_2 + m \sum_{\text{bound}} \mathbf{v}_i = 0, \quad (21)$$

where \mathbf{V}_2 and \mathbf{v}_i are the velocity of the black hole and of a bound star with respect to the center of mass of the bound system. Ignoring correlations between the motions of the bound stars, we find

$$\langle V_2^2 \rangle = \frac{3M_b m}{M^2} \sigma_b^2 \quad (22)$$

with σ_b the velocity dispersion of the bound stars.

Combining the two pieces gives

$$\langle V^2 \rangle \approx \frac{3m}{M} \left(\frac{M}{M+M_b} \sigma_u^2 + \frac{M_b}{M} \sigma_b^2 \right). \quad (23)$$

Since $M_b \approx M$, this is roughly

$$\langle V^2 \rangle \approx \frac{3m}{M} \left(\frac{\sigma_u^2}{2} + \sigma_b^2 \right). \quad (24)$$

For $F' \approx 1$, σ_b is of the same order or greater than σ_u for most (γ, M) , hence the quantity in parentheses on the right hand side of equation (24) is comparable to $\tilde{\sigma}^2$. Thus our model naturally reproduces the dependence of $\langle V^2 \rangle$ observed in the N -body simulations.

Figure 7 shows predicted values of $\langle V^2 \rangle$ for $F' = 1$. The match with the data in Figure 4 is quite good.

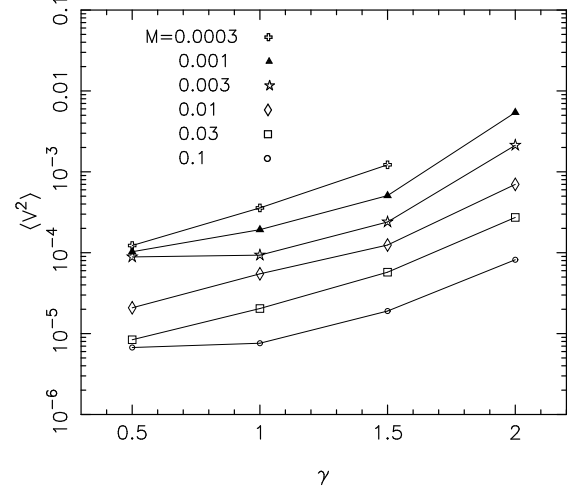


FIG. 5.— Mean square velocity of the black hole particle for the N -body integrations listed in Table 2. These are the same data as in Figure 4, but plotted to show the dependence on γ .

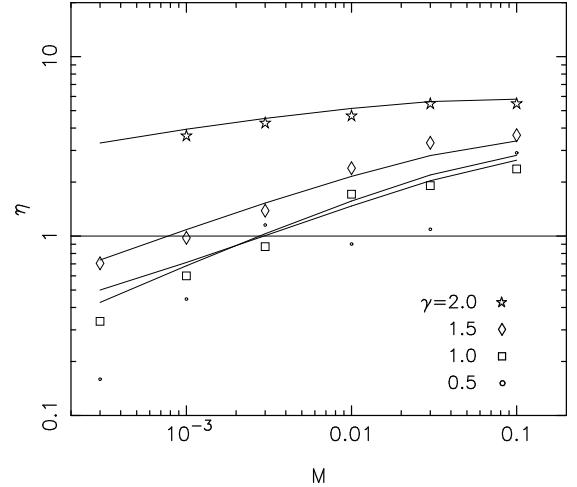


FIG. 6.— The quantity η (equation 15) that measures departures from “equipartition” in the N -body models. Lines are the values of η predicted if the black hole is assumed to be in energy equipartition with stars lying at distances $\leq 0.6r_h$ from it.

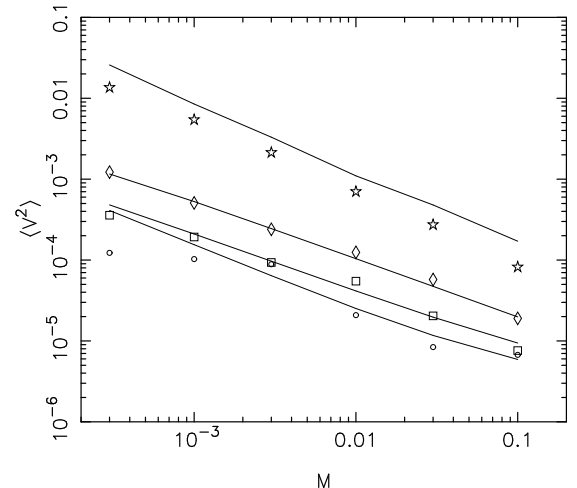


FIG. 7.— Predicted values of $\langle V^2 \rangle$ based on the model of §5. Symbols show the N -body data, as in Figure 4.

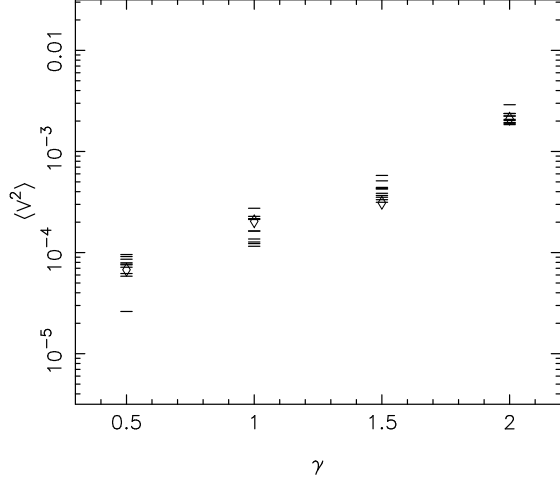


FIG. 8.— Mean square black hole velocity in the multi-mass integrations. For each value of M , ten N -body integrations were carried out using different seeds for the random number generator for the stellar masses; the results for each integration are indicated by —. The \diamond symbols show the predicted values based on the theory in §4.

6. RESULTS: MULTI-MASS MODELS

Stars in real galaxies do not all have the same mass. We carried out an additional set of N -body integrations based on the same galaxy models as before, but generating the mass of each “star” particle from a Salpeter (1955) mass function,

$$n(m)dm \propto m^{-(1+\alpha)}dm, \quad m_1 \leq m \leq m_2, \quad (25)$$

with $\alpha = 1.35$. We chose $m_2/m_1 = 100$; the values of m_1 and m_2 are then fixed by the requirement that the mean stellar mass equal N^{-1} . Each of these integrations used $M = 10^{-2}$ and $N = 10^6$. Because these galaxy models contain a small number of massive stars (those at the high-mass tail of the distribution), we expect the statistical variance of the results to be greater than in the single-mass runs. Hence we carried out 10 integrations of each model using different seeds to initialize the random number generator for the stellar masses. The $\langle V^2 \rangle$ values given in Table 4 are averages over these 10 runs. We also used shorter integration times than in the single-mass integrations in order to reduce the effects of mass segregation: $T = (2, 1, 0.5, 0.25)$ for $\gamma = (0.5, 1, 1.5, 2)$ respectively. We give in Table 4 $\sigma_{\langle V^2 \rangle}$, the variance in the measured $\langle V^2 \rangle$ values for the 10 runs, and ratio between the mean $\langle V^2 \rangle$ and the value measured in the single-mass runs for the same (γ, M, N) . We computed the latter quantities over the same time intervals used for the multi-mass integrations.

As shown in §4, Chandrasekhar’s theory allows us to predict a relation between the black hole’s mean square velocity in the multi-mass and single-mass cases. The former is predicted to be larger than the latter by a factor \tilde{m}/m , where \tilde{m} is defined in equation (13). Substituting equation (25) into equation (13) gives

$$\tilde{m} = \left(\frac{1-\alpha}{2-\alpha} \right) m_1 \left[\frac{\left(\frac{m_2}{m_1} \right)^{2-\alpha} - 1}{\left(\frac{m_2}{m_1} \right)^{1-\alpha} - 1} \right]. \quad (26)$$

Setting $\alpha = 1.35$ and $m_2/m_1 = 100$ yields $\tilde{m} = 12.7m_1 = 4.10\bar{m}$ where $\bar{m} = N^{-1}$ is the mean stellar mass. Hence, in the multi-mass integrations, Chandrasekhar’s theory predicts

TABLE 4
MULTI-MASS N -BODY INTEGRATIONS

γ	$\langle V^2 \rangle$	$\sigma_{\langle V^2 \rangle}$	ratio
0.5	6.58×10^{-5}	2.8×10^{-5}	3.98
1.0	1.60×10^{-4}	7.0×10^{-5}	3.22
1.5	3.77×10^{-4}	1.4×10^{-4}	4.98
2.0	1.99×10^{-3}	6.9×10^{-4}	3.87

a mean square velocity for the black hole that is roughly four times larger than in the single-mass integrations.

The final column of Table 4 gives the measured values of this ratio, and Figure 8 shows the 10 measured values of $\langle V^2 \rangle$ for each value of γ , compared with 4.1 times the measured value in the corresponding single-mass run. While the variation from run to run is large, the mean increase in $\langle V^2 \rangle$ is reasonably close to the predicted factor.

7. DISCUSSION

Our N -body integrations show that a black hole at the center of a dense stellar system responds to perturbations from passing stars by achieving a time-averaged kinetic energy given by

$$\frac{1}{2}M\langle V^2 \rangle \approx \frac{3}{2}\tilde{m}\tilde{\sigma}^2 \quad (27)$$

where $\tilde{\sigma}^2$ is the 1D, mean square stellar velocity within a region $r \lesssim 0.6r_h$ around the black hole, r_h is the black hole’s influence radius (defined as the radius containing a mass in stars equal to twice the black hole’s mass), and \tilde{m} is an effective stellar mass defined via equation (13); in the case of a delta-function mass spectrum, \tilde{m} is equal to the stellar mass. Equation (27) was found to provide a reasonably accurate description of the N -body integrations in galaxy models with power-law nuclei, $\rho \propto r^{-\gamma}$, $0.5 \leq \gamma \leq 2$, and for black hole masses in the range $10^{-4} \leq M/M_{gal} \leq 10^{-1}$. A more accurate description of the N -body results is given by equation (15) (with m replaced by \tilde{m}) and Table 3, or simply by the measured values in Tables 2. The detailed distribution of black hole velocities, $N(V)$, was found to be essentially indistinguishable from a Maxwell-Boltzmann distribution (Figure 3).

As discussed above (§5), equation (27) has a simple physical interpretation: the presence of the black hole deepens the galaxy’s central potential and increases the velocities of stars in its vicinity, and these high-velocity stars provide in turn the dominant perturbations that determine the amplitude of the black hole’s Brownian velocity. The dependence of $\langle V^2 \rangle$ on M is therefore less steep than M^{-1} , since increasing M also increases the velocities of nearby stars.

If we accept equation (27), it is straightforward to derive simple analytic expressions for the dependence of $\langle V^2 \rangle$ on M/M_{gal} and γ . For the Dehnen models studied here, the black hole’s influence radius is given by

$$r_h = \frac{(2M)^{1/(3-\gamma)}}{1 - (2M)^{1/(3-\gamma)}} \approx (2M)^{\frac{1}{(3-\gamma)}}, \quad M \ll 1 \quad (28)$$

in model units ($G = M_{gal} = a = 1$). The quantity $\tilde{\sigma}^2$ that appears in equation (27) is defined as a number-weighted mean within a distance $F \times r_h$ from the black hole, where $F \approx 0.6$ (§5). Here we can make use of the analytic expressions for

$\sigma^2(r)$ given by Dehnen (1993) and Tremaine et al. (1994). We write

$$\sigma^2(r) = \sigma_1^2(r) + M\sigma_2^2(r) \quad (29)$$

where σ_1^2 is the contribution to σ^2 from the stellar potential, and σ_2^2 is the additional component due to the presence of the black hole. For $1 < \gamma \leq 2$ and at radii $\lesssim r_h$, we have

$$\sigma_1^2(r) \approx \frac{r^{2-\gamma}}{2(\gamma-1)}, \quad \sigma_2^2(r) = \frac{M}{(1+\gamma)} \frac{1}{r}. \quad (30)$$

Averaging over a sphere of radius Fr_h , and expressing the result in physical units, we find

$$\tilde{\sigma}^2 \approx H(\gamma, F) \left(\frac{GM_{gal}}{a} \right) \left(\frac{M}{M_{gal}} \right)^{(\gamma-2)/(\gamma-3)}, \quad (31a)$$

$$H(\gamma, F) = 2^{1/(\gamma-3)} (3-\gamma) F^{-1} \left[\frac{(1+\gamma)(2-\gamma)F^{3-\gamma} + (\gamma-1)(5-2\gamma)}{(\gamma^2-1)(5-2\gamma)(2-\gamma)} \right]. \quad (31b)$$

(Note the divergence when $\gamma = 2$, discussed in §5.) Setting $F = 0.6$ (§5) gives $H \approx 2.3 \pm 0.4$ for γ in the range $1.2 \leq \gamma \leq 1.8$. The black hole's mean square velocity is then predicted to be, via equation (27),

$$\langle V^2 \rangle \approx 7 \left(\frac{GM_{gal}}{a} \right) \left(\frac{\tilde{m}}{M_{gal}} \right) \left(\frac{M_{gal}}{M} \right)^{1/(3-\gamma)}, \quad 1 \lesssim \gamma \lesssim 2. \quad (32)$$

When translated back into model units, this is $\langle V^2 \rangle \approx 7N^{-1}M^{-1/(3-\gamma)}$, which is a tolerable fit to the $\langle V^2 \rangle$ values plotted in Figures 4 and 7. The analytic expressions for $\langle V^2 \rangle$ when γ is in the range $0.5 \leq \gamma \leq 1$ are more complicated but still imply $\langle V^2 \rangle \propto M^{-1/(3-\gamma)}$ for small M/M_{gal} .

The fact that $\langle V^2 \rangle$ falls off less steeply than M^{-1} with increasing mass is perhaps the first clear indication that gravitational Brownian motion differs in a significant way from its fluid analog, for which $\langle V^2 \rangle \propto M^{-1}$. It would be of interest to refine the M -dependence. Extending the N -body integrations to longer times would reduce the noise but increase the possibility of systematic errors due to collisional evolution of the models. An alternative would be to carry out a large number of shorter integrations and average the results, as was done here in the multi-mass studies (§6).

When making predictions about the expected amplitude of the Brownian velocity of black holes in real galaxies, an expression like equation (32) is not ideal since it contains the terms M_{gal} and a that depend on the large-radius properties of the galaxy. A less model-dependent way to present these results is in terms of the central properties of the galaxy. Here we return to equation (15) and to the empirical relation established between η and M :

$$\langle V^2 \rangle = 3\eta \frac{\tilde{m}}{M} \sigma_p^2, \quad (33a)$$

$$\log_{10} \eta \approx A + B \log_{10} M \quad (33b)$$

where the best-fit coefficients A and B as derived from the N -body integrations are given in Table 3. Equations (33) give $\langle V^2 \rangle$ in terms of σ_p , the peak value of σ measured outside of the black hole's influence radius (Figure 1, Table 1). This quantity is easily accessible via ground-based observations for many galaxies.

As an example, we consider the nucleus of the Milky Way. The peak velocity dispersion is $\sigma_p \approx 150 \text{ km s}^{-1}$

(Kent 1992). For the stellar density profile at the center of the Milky Way bulge, Genzel et al. (2003) find $\rho \propto r^{-\gamma}$ with $\gamma \approx 1.4 \pm 0.1$, consistent with the value $\gamma = 1.5$ used here in some of the N -body integrations. Finally, the black hole mass is $3.4 \pm 0.5 \times 10^6 M_\odot$ (Schödel et al. 2003). Since the Milky Way black hole falls on the tight scaling relations defined by the other secure black hole masses (Ferrarese & Merritt 2000; Marconi & Hunt 2003), we assume that $M/M_{gal} \approx 1.25 \times 10^{-3}$, the mean ratio of black hole mass to bulge mass defined by these galaxies (Merritt & Ferrarese 2001). From Table 4 or Figure 6, we then have $\eta \approx 1.5$ and

$$V_{rms} \approx 0.17 \text{ km s}^{-1} \left(\frac{\tilde{m}}{1M_\odot} \right)^{1/2} \left(\frac{M}{3.4 \times 10^6 M_\odot} \right)^{-1/2} \times \left(\frac{\sigma_p}{150 \text{ km s}^{-1}} \right). \quad (34)$$

The characteristic stellar mass \tilde{m} (equation 13) depends on the poorly-known mass function for stars in the Galactic nucleus but \tilde{m} is probably of order M_\odot (Genzel et al. 2003). Hence we predict $V_{rms} \approx 0.2 \text{ km s}^{-1}$.

Current limits on the motion of the Milky Way black hole are based on proper motion measurements of images of Sagittarius A* ($V_{pm} \lesssim 8 \text{ km s}^{-1}$; Reid et al. (2003)). Such measurements require observations over an extended period of time; in the case of the Reid et al. (2003) study, the baseline was ~ 7 yr. The measured velocity is derived from the integrated displacement. If the black hole's velocity changes significantly during this time, the distribution of measured velocities will be different than the distribution of instantaneous velocities. To evaluate the importance of this effect for proper motion measurements in the Galactic center, we used our N -body results to compute displacements of the black hole particle over finite times, then computed distributions of the proper motion velocities that would be measured from these displacements. (We note that the time scale over which the massive particle's velocity changes is predicted to be *independent* of the number of perturbers for a given mean perturber density, based on the equations in §4.) After scaling to the Galactic center, we found almost no dependence of the measured (proper motion) velocities on the measurement baseline, for times up to $\sim 10^3$ yr. We therefore base the following discussion on the instantaneous velocity distribution $N(V)$.

Given that $N(V)$ is expected to be a Maxwell-Boltzmann distribution (equation 14), we can use the estimate of V_{rms} to compute the probability that a random velocity measurement will exceed any value V_0 . We first convert the velocity distribution of equation (14) into a distribution over 2D velocities V_{pm} in the plane of the sky. Transforming, we find

$$N(V_{pm})dV_{pm} = (\langle V^2 \rangle / 3)^{-1} V_{pm} e^{-3V_{pm}^2/2\langle V^2 \rangle} dV_{pm}. \quad (35)$$

The probability of measuring V_{pm} to be greater than V_0 , given $\langle V^2 \rangle$, is then just $\exp(-3V_0^2/2\langle V^2 \rangle)$. If $\langle V^2 \rangle = (0.17 \text{ km s}^{-1})^2$, the expected value for the Milky Way black hole, the probability that V_{pm} will exceed $V_0 = (0.1, 0.2, 0.3, 0.4, 0.5) \text{ km s}^{-1}$ is $(0.60, 0.13, 9.4 \times 10^{-3}, 2.5 \times 10^{-4}, 2.3 \times 10^{-6})$. In order to have a reasonable chance of detecting the black hole's motion, a velocity resolution better than 0.3 km s^{-1} will be required.

Once a bona fide measurement of V_{pm} has been made, the black hole's velocity can be converted into an estimate of its

mass. Here we make use of Bayes's theorem:

$$P(M|V_{pm}) = \frac{P(M)P(V_{pm}|M)}{\int dM' P(M')P(V_{pm}|M')}. \quad (36)$$

where $P(a|b)da$ denotes the probability, given b , of measuring a in the range a to $a + da$, and $P(M)dM$ is the prior probability that M lies in the range M to $M + dM$. Here “prior” means “given all knowledge prior to the measurement of V_{pm} .” A completely uninformed prior would be $P(M) = \text{constant}$; another standard choice is $P(M) \propto M^{-1}$; and of course one could use information about M from other sources (e.g. Schödel et al. (2003)) to construct even more informed priors.

Adopting the maximally-uninformed prior, and using equations (33) and (35) to write $P(V_{pm}|M)$, we find the probability distribution of M given a measured $V_{pm} = V_0$ to be

$$P(M|V_0)dM = \frac{V_0^4}{4\tilde{m}^2\eta^2\sigma_p^4} M e^{-MV_0^2/2\tilde{m}\eta\sigma_p^2} dM \quad (37)$$

and the probability that $M \geq M_0$ is

$$P(M \geq M_0|V_0) = \left(1 + \frac{M_0 V_0^2}{2\tilde{m}\eta\sigma_p^2}\right) e^{-M_0 V_0^2/2\tilde{m}\eta\sigma_p^2}. \quad (38)$$

(In deriving these equations we have ignored the relatively weak dependence of η on M , Table 4. Including that dependence is straightforward but results in non-analytic expressions for P .) We define the “best estimate” \mathcal{M} of the black hole's mass to be the median value from this distribution. This is

$$\mathcal{M} = \frac{3.36\tilde{m}\eta\sigma_p^2}{V_0^2}. \quad (39)$$

We propose to call this the “Brownian mass estimator.” For the Milky Way black hole ($\sigma_p \approx 150 \text{ km s}^{-1}$, $\eta \approx 1.5$), the estimated mass is

$$\mathcal{M} \approx 2.8 \times 10^6 M_\odot \left(\frac{\tilde{m}}{1M_\odot}\right) \left(\frac{V_0}{0.2 \text{ km s}^{-1}}\right)^{-2}. \quad (40)$$

The 90% confidence intervals on the mass are given by the values of M_0 for which $P(M \geq M_0|V_0) = (0.05, 0.95)$, or

$$0.211\mathcal{M} \leq M \leq 2.82\mathcal{M}. \quad (41)$$

Unlike mass estimators based on the statistics of a large sample, the uncertainty associated with Brownian mass estimators is irreducible, and it probably makes more sense to interpret a measured V_{pm} as defining a probability distribution for M via equation (38) than a most-likely value via equation (40). For example, if V_{pm} for the Milky Way black hole were measured to be 0.1 km s^{-1} , the probability that its mass exceeds $(10^6, 10^7, 10^8)M_\odot$ would be (99.0%, 56.4%, 0.00058%).

Figure 9 plots $P(M|V_0)$ in the case of the Milky Way black hole ($\sigma_p = 150 \text{ km s}^{-1}$, $\eta = 1.5$) for four values of V_0 . Also shown (by tick marks) are the median values \mathcal{M} .

If we adopt instead the “informed” prior, $P(M) \propto M^{-1}$, then

$$P(M|V_0)dM = \frac{V_0^2}{2\tilde{m}\eta\sigma_p^2} e^{-MV_0^2/2\tilde{m}\eta\sigma_p^2}, \quad (42a)$$

$$P(M \geq M_0|V_0) = e^{-M_0 V_0^2/2\tilde{m}\eta\sigma_p^2} \quad (42b)$$

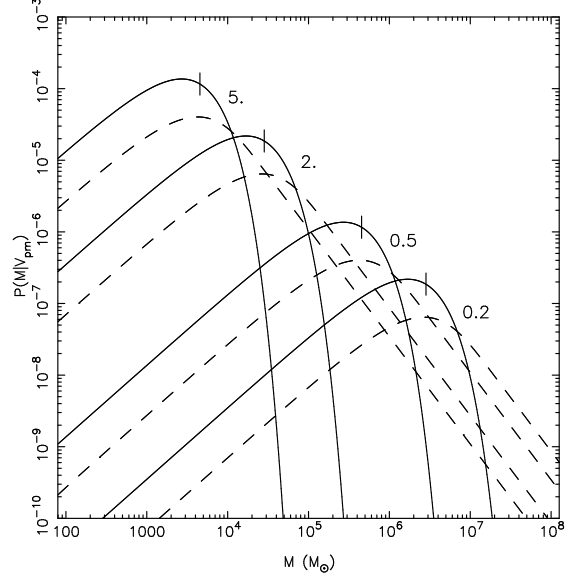


FIG. 9.— Probability distribution for the mass of the Milky Way black hole, based on measurement of a proper motion velocity (solid curves), or based on determination of an upper limit to the proper-motion velocity (dashed curves), for four values of V_{pm} in km s^{-1} . Tick marks indicate median values.

and the Brownian mass estimator becomes

$$\mathcal{M} = \frac{1.39\tilde{m}\eta\sigma_p^2}{V_0^2} \approx 1.2 \times 10^6 M_\odot \left(\frac{\tilde{m}}{1M_\odot}\right) \left(\frac{V_0}{0.2 \text{ km s}^{-1}}\right)^{-2}. \quad (43)$$

The median mass is now smaller due to the prior which disfavors high masses.

Finally, we ask what can be learned about the black hole mass if only an upper limit on its velocity, $V_{pm} \leq V_{up}$, is available. We consider the determination of an upper limit on V_{pm} to be equivalent to the statement that any velocity in the interval $0 \leq V_{pm} \leq V_{up}$ is equally likely, and that velocities greater than V_{up} have zero probability. The probability distribution for the mass is then

$$P(M|V \leq V_{up}) = \frac{\int_0^{V_{up}} P(M|V_0) dV_0}{\int_0^{V_{up}} dV_0}. \quad (44)$$

Again adopting the uninformed prior for $P(M)$, we find

$$P(M|V \leq V_{up}) = \frac{1}{8M} \frac{\mathcal{V}}{V_{up}} \left\{ 3\sqrt{\pi} \text{erf}\left(\frac{V_{up}}{\mathcal{V}}\right) - 2e^{-V_{up}^2/\mathcal{V}^2} \times \left[\frac{V_{up}}{\mathcal{V}} \left(3 + 2\frac{V_{up}^2}{\mathcal{V}^2} \right) \right] \right\} \quad (45)$$

with

$$\mathcal{V}^2(M) = \frac{2\tilde{m}\eta\sigma_p^2}{M}. \quad (46)$$

This function is plotted in Figure 9 for various V_{up} , using the same values of \tilde{m} and σ_p given above for the Milky Way. The low- M tail of the distribution is similar to that of $P(M|V_0)$, but there is a more extended tail at high M corresponding to the fact that low values of V_{pm} are (by assumption) equally as likely as V_{up} .

We thank the anonymous referee for comments that substantially improved this paper. This work was supported

by grants AST-0206031, AST-0420920 and AST-0437519 from the NSF, grant NNG04GJ48G from NASA, grant HST-AR-09519.01-A from STScI, grant I/80 041 GRACE from the Volkswagen Foundation, by SFB439 of Deutsche

Forschungsgemeinschaft, and by INTAS grant IA-03-59-11. We thank the Center for the Advancement of the Study of Cyberinfrastructure at RIT for their support.

REFERENCES

- Backer, D. C. & Sramek, R. A. 1999, *ApJ*, 524, 805
Bahcall, J. N. & Wolf, R. A. 1976, *ApJ*, 209, 214
Berczik, P., Merritt, D. & Spurzem, R. 2005, *ApJ*, 633, 680
Chatterjee, P., Hernquist, L. & Loeb, A. 2002a, *ApJ*, 572, 371
Chatterjee, P., Hernquist, L. & Loeb, A. 2002b, *PRL* 88, 121103
Chatterjee, P., Hernquist, L. & Loeb, A. 2003, *ApJ*, 592, 32
Dehnen, W. 1993, *MNRAS*, 265, 250
Dorband, E. N., Hemsendorf, M., & Merritt, D. 2003, *J. Comp. Phys.*, 185, 484
Ferrarese, L. & Merritt, D. 2000, *ApJ*, 539, L9
Fukushige, T., Makino, J. & Kawai, A. 2005, *PASJ*, 57, 1009
Genzel, R. et al. 2003, *ApJ*, 594, 812
Kent, S. M. 1992, *ApJ*, 387, 181
Laun, F. 2004, Masters Thesis, Rutgers University
Lightman, A. P. & Shapiro, S. L. 1977, *ApJ*, 211, 244
Makino, J. & Aarseth, S. J. 1992, *PASJ*, 44, 141
Makino, J. & Funato, Y. 2004, *ApJ*, 602, 93
Maoz, E. 1993, *MNRAS*, 263, 75
Marconi, A. & Hunt, L. K. 2003, *ApJ*, 589, L21
Merritt, D. 2001, *ApJ*, 556, 245
Merritt, D. 2004, preprint (astro-ph/0405351)
Merritt, D. 2005, *ApJ*, 628, 673
Merritt, D. & Ferrarese, L. 2001, *MNRAS*, 320, L30
Miller, R. H. 1992, *ApJ*, 393, 508
Milosavljević, M. & Merritt, D. 2001, *ApJ*, 563, 34
Preto, M., Merritt, D. & Spurzem, R. 2004, preprint (astro-ph/0406324)
Reid, M. J., Readhead, A. C. S., Vermeulen, R. C., & Treuhaft, R. N. 1999, *ApJ*, 524, 816
Reid, M. J., Menten, K. M., Genzel, R., Ott, T., Schödel, R., & Brunthaler, A. 2003, *Astron. Nachr.* 324, No. S1, 3
Salpeter, E. E. 1955, *ApJ*, 121, 161
Schödel, R. et al. 2003, *ApJ*, 596, 1015
Spitzer, L. 1987, *Dynamical Evolution of Globular Clusters* (Princeton: Princeton University Press), 40
Taga, M. & Iye, M. 2008, *MNRAS*, 390, 111
Tremaine, S. et al. 1994, *AJ*, 107, 634
Young, P. J. 1980, *ApJ*, 215, 36